Applied Geochemistry 27 (2012) 151–160

Contents lists available at SciVerse ScienceDirect

Applied Geochemistry

journal homepage: www.elsevier.com/locate/apgeochem

Metallogeny and environmental impact of Hg in Zn deposits in China

Runsheng Yin [a,b], Xinbin Feng [a,*], Zhonggen Li [a], Qian Zhang [c], Xianwu Bi [c], Guanghui Li [a,b], Jinling Liu [a,b], Jingjing Zhu [b,c], Jianxu Wang [a,b]

[a] State Key Laboratory of Environmental Geochemistry, Institute of Geochemistry, Chinese Academy of Sciences, Guiyang 550002, China
[b] Graduate University of the Chinese Academy Sciences, Beijing 100039, China
[c] State Key Laboratory of Ore Deposit Geochemistry, Institute of Geochemistry, Chinese Academy of Sciences, Guiyang 550002, China

ARTICLE INFO

Article history:
Received 11 April 2011
Accepted 23 September 2011
Available online 29 September 2011
Editorial handling by B. Wang

ABSTRACT

Zinc smelting is currently regarded as one of the most important atmospheric Hg emission sources in the world. In order to assess the potential environmental impacts of Hg from Zn smelting in China, the distribution of total Hg concentration (HgT) in Zn concentrates (ZCs) from 100 Zn deposits in China was investigated. It was found that HgT varies depending on the ore types and their geneses. Zinc concentrates from sedimentary-exhalative deposits (SEDEX, geometric mean = 48.2 μg/g) have the highest HgT. The possible explanation is that the sources of mineralizing solutions for SEDEX deposits are deep formational brines in contact with sedimentary rocks, and there are much higher background Hg contents in sedimentary rocks. Zinc concentrates from volcanic hosted massive sulfide deposits (VMS, geometric mean = 11.5 μg/g) and Mississippi Valley-Type (MVT, geometric mean = 10.1 μg/g) deposits have intermediate HgT. VMS may receive most of their Hg from fluid–rock interaction and/or by direct input of gaseous Hg from a mantle source. However, the source of metals within MVTs may be the low-temperature hydrothermal solution formed by diagenetic recrystallization of the carbonates. Intrusion related deposits (IRs) have the lowest HgT (Geomean = 2.4 μg/g), and the dispersion of Hg in the IRs seems to be influenced by the temperature of ore formation and/or the nature of wall–rock alteration. Finally, it was estimated that the annual Hg emission to the atmosphere from Zn smelting in China was about 107.7 tons in 2006.

1. Introduction

China is rich in Zn resources and the reserve of Zn ores ranks second in the world. The Zn production in China, which accounted for more than 25% of the global production in 2006, has ranked first in the world since 2002 (ECCNMY, 2003–2007; Jiang, 2004). Since both Hg and Zn are chalcophile elements, Hg is commonly distributed in most mineral deposit types that contain Zn. Zinc occurs mainly as independent minerals in nature and is typically closely associated with sphalerite (Ozerova et al., 1975). Zn smelting releases several hundred tons of Hg into the environment each year worldwide (Nriagu and Pacyna, 1988; Streets et al., 2005; Pacyna et al., 2006). Mercury emission from Zn smelting in the developed countries is well controlled due to the installation of Hg removal facilities, but in developing countries Hg emission from Zn smelting could be substantial simply due to lack of control (Streets et al., 2005; Li et al., 2010).

The total Hg concentration (HgT) of Zn concentrates (ZCs) is not solely an environmental problem. The characteristic of relatively high vapor pressures of Hg compounds enhances their hypogene mobility during mineralization (Fursov, 1958; McCarthy, 1972). Theoretical and experimental studies have confirmed the ability of Hg as a transporting agent of ore metals during hydrothermal mineralization (Holland, 1972; Kilinc and Burnham, 1972). Furthermore, the volatile property of Hg has led to it being widely utilized as a potential pathfinder in geochemical prospecting for geothermal energy (Zhu et al., 1986), a wide variety of base and precious metal deposits, such as Au deposits (Nelson, 1990), U deposits (You and Li, 1990) and W–Mo deposits (Garrett, 1974), as well as base-metal deposits (Fedikow and Amor, 1990).

Previous studies have demonstrated that HgT in Zn ores is highly variable, depending on ore type, origin or geneses, and location (Schwartz, 1997). China has undergone multiple tectonic and magmatic events that have resulted in a variety of metallogenic processes since the Archean (Zhai and Deng, 1996). The complex tectonic background has strongly influenced and in many cases controlled the types and locations of Zn mineralization as shown in Fig. 1. In China, Zn mineralization mainly occurs as four subtypes, namely: sedimentary-exhalative deposits (SEDEX), Mississippi Valley-Type (MVT), volcanic hosted massive sulfides (VMS) and intrusion related (IR) types (Dai et al., 2005). In this paper, a

* Corresponding author.
E-mail address: fengxinbin@vip.skleg.cn (X. Feng).

0883-2927/$ - see front matter © 2011 Elsevier Ltd. All rights reserved.
doi:10.1016/j.apgeochem.2011.09.027

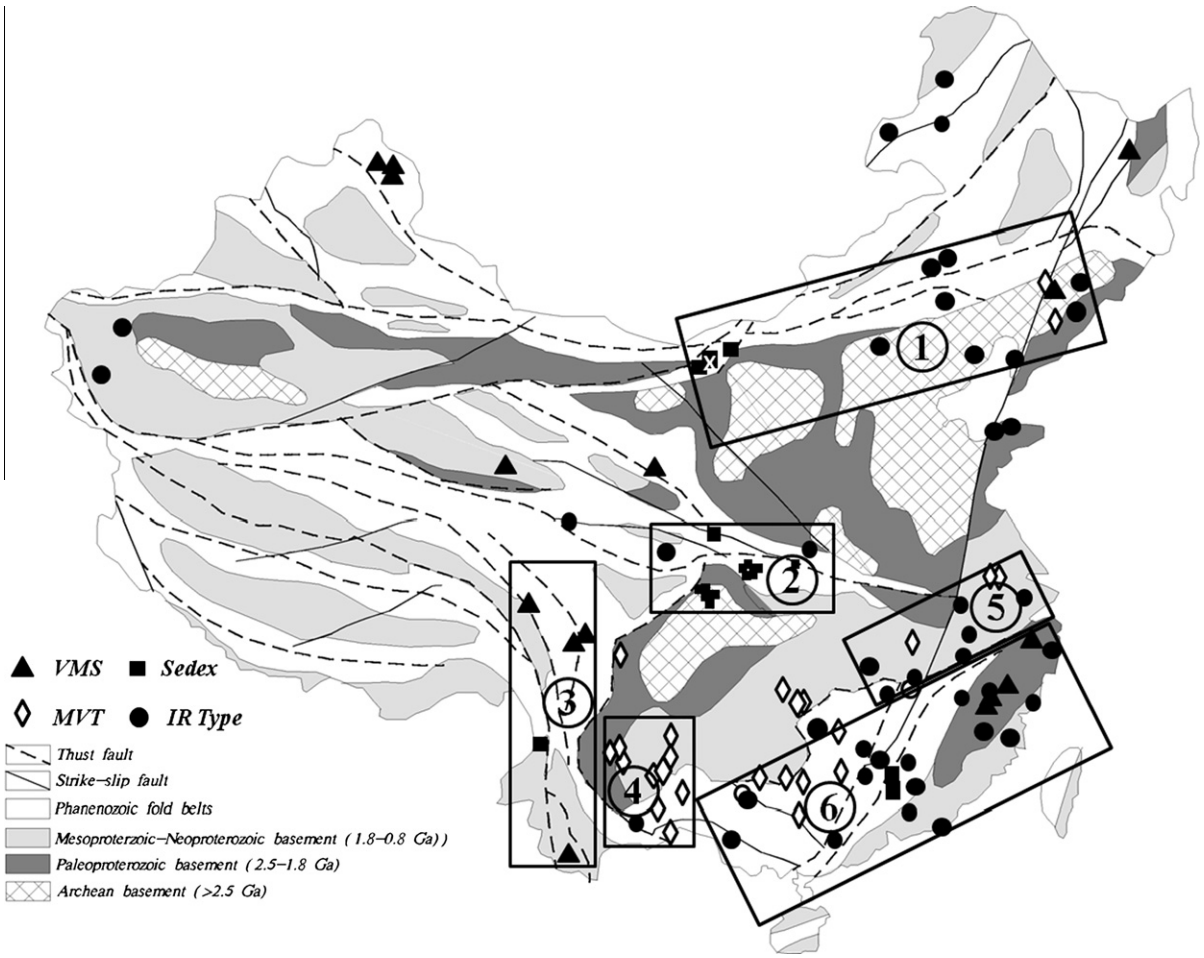

Fig. 1. Tectonic partitioning and sampling locations of Zn deposits in China. Major Zn metallogenic belts are summarized as: (1) the northern margin of the North China Craton, (2) Kunlun-Qinling Belt, (3) the Sanjiang fold belt covering eastern Tibet, Sichuan and Yunnan, (4) the Kangdian Belt, (5) the Lower to Middle Yangtze River belt covering Hunan, Hubei, Anhui and Jiangsu, and (6) the Nanling Mountain belt of the South China fold belt (Dai et al., 2005).

comprehensive investigation of HgT in 100 deposits in China has been investigated. The main goals of this study were (1) to investigate the potential dependence of HgT on ore type and genesis of Zn deposits and (2) to estimate Hg emissions from Zn smelting in China.

2. Experimental section

2.1. Tectonic settings and Zn metallogeny history in China

China consists of a complex amalgamation of tectonic blocks, and the geology of China reflects long-continued development, evolution, amalgamation and renewed tectonism of cratonic blocks and mobile belts (Wang, 1993). The complexity of the geological evolution of China has resulted in formation of a series of Zn mineral deposits as shown in Fig. 1. From the Archean to the early Late Proterozoic a number of discrete cratonic blocks developed (Wang, 1993). The Late Proterozoic to early Mesozoic was mainly an interval of continental margin development followed by drifting of these blocks across the Tethyan Ocean (Yang, 1998). The mid-Mesozoic to the Cenozoic was mainly an interval of intracontinental deformation and circum-Pacific orogeny (Shen, 2000). The Proterozoic era was one of the important metallogenic periods for the formation of VMS and SEDEX mineralization in China. During this era, aulacogens and rifts were developed in the interior and on some margins of the three cratons (North China Craton, Tarim Craton and Yangtze Craton). In the late Paleozoic the Siberian and Tarim-North China plates amalgamated. A number of SEDEX deposits were formed. Synsedimentary faults played an important role in the formation of these SEDEX deposits (Zeng and Shen, 1987). In the Paleozoic, along the western margin of the Yangtze Craton (the Kangdian Belt), an Early Carboniferous sequence of marine-facies carbonate rocks hosts a number of MVT deposits. In the early Mesozoic the Tarim-North China plate merged with the Yangtze Craton. In the early Cenozoic the final closure of the Tethian oceans occurred, bringing about suturing of the Indian and Tibet–Yunnan plates (Yang, 1998; Shen, 2000). The country can be divided into two major tectonic provinces. In the east, the interaction between the continent of East Asia and the Pacific plate resulted in extensive volcanic and intrusive activity in the Pacific margin tectonic belt and the formation of continental sedimentary basins (Ren et al., 1990). The extensive Jurassic–Cretaceous continental volcanic and intrusive activity led to the development of many types of mineral deposits, especially for the intrusion related (IR) types as shown in Fig. 1. The volcanic rocks, which are distributed along NNE-trending fractures, were characterized by the tectono-magmatic activity related to the Yanshanian magmatism (Wang, 1993). In the west, all the terrains in the Qinghai-Tibet area, formerly belonging to Gondwanaland, were accreted to the Eurasia plate. The Indian plate collided and sutured with the Eurasian plate during the Cenozoic Himalayan movement resulting in the

Table 1
HgT concentrations in SEDEX zinc deposits.

Deposit no.	Deposit name	Locations	Provinces	Host ages	HgT (μg/g)	Zn (10^4 tons)	ZC (10^4 tons)	HgR (t)	Deposit types
S-1	Jiashengpan	Wulate	Neimenggu	Proterozoic	5.49	126.85	317.13	17.41	SEDEX
S-2	Dongshengmiao	Wulate	Neimenggu	Proterozoic	7.03	408.24	1020.6	71.75	SEDEX
S-3	Tanyaokou	Wulate	Neimenggu	Proterozoic	3.16	110.66	276.65	8.74	SEDEX
S-4	Dabaoshan	Qujiang	Guangdong	Yanshanian	5.17	69.79	174.48	9.02	SEDEX
S-5	Jinding	Lanping	Yunnan	Himalayan	29.78	1347.07	3367.68	1002.89	SEDEX
S-6	Qiandongshan	Fengxian	Shanxi	Hercynian	71.9	91.81	229.53	165.03	SEDEX
S-7	Bafangshan	Fengxian	Shanxi	Hercynian	9.31	39.74	99.35	9.25	SEDEX
S-8	Yinmusi	Fengxian	Shanxi	Hercynian	141	21.43	53.58	75.54	SEDEX
S-9	Fengya	Fengxian	Shanxi	Hercynian	91	28.46	71.15	64.75	SEDEX
S-10	Erlihe	Fengxian	Shanxi	Hercynian	191	27.33	68.33	130.5	SEDEX
S-11	Yindongliang	Fengxian	Shanxi	Hercynian	89	32.99	82.48	73.4	SEDEX
S-12	Yindongzi	Zuoshui	Shanxi	Hercynian	5.59	0.99	2.48	0.14	SEDEX
S-13	Changba	Chengxian	Gansu	Hercynian	195	306.44	766.10	1493.9	SEDEX
S-14	Lijiagou	Chengxian	Gansu	Hercynian	300	164.41	411.03	1233.08	SEDEX
S-15	Bijiashan	Chengxian	Gansu	Hercynian	91.7	45.92	114.8	105.27	SEDEX
S-16	Dengjiashan	Xihe	Gansu	Hercynian	210	46.49	116.23	244.07	SEDEX
S-17	Luoba	Huixian	Gansu	Hercynian	323	88.10	220.25	711.41	SEDEX
S-18	Jiaolongzhang	Langzhuang	Gansu	Caledonian	72.37	13.79	34.48	24.95	SEDEX
S-19	Fankou	Renhua	Guangdong	Yanshanian	237	549.28	1373.20	3254.48	SEDEX

Additional reference, Dai et al., 2005.

Table 2
HgT concentrations in VMS zinc deposits.

Deposit no.	Deposit name	Locations	Provinces	Host ages	HgT (μg/g)	Zn (10^4 tons)	ZC (10^4 tons)	MR (t)	Deposit types
V-1	Hongtoushan	Qingyuan	Liaoning	Archean	179.7	68.84	172.10	309.26	VMS
V-2	Wuao	Longquan	Zhejiang	Yanshanian	10.74	16.74	41.85	4.49	VMS
V-3	Qiwan	Zhuji city	Zhejiang	Yanshanian	111.60	11.40	28.50	31.81	VMS
V-4	Shuiji	Jianyang	Fujian	Proterozoic	2.97	24.15	60.375	1.79	VMS
V-5	Meixian	Youxi	Fujian	Proterozoic	11.25	87.44	218.60	24.59	VMS
V-6	Jiacun	Baiyu	Sichuan	Indosinian	2.28	86.73	216.83	4.94	VMS
V-7	Gayiqiong	Baiyu	Sichuan	Indosinian	10.47	31.33	78.325	8.20	VMS
V-8	Xiaotieshan	Baiyin	Gansu	Proterozoic	117.6	64.18	160.45	188.69	VMS
V-9	Xitieshan	Chaidamu	Qinghai	Caledonian	96.00	181.72	454.30	436.13	VMS
V-10	Zhaokalong	Yushu	Qinghai	Indosinian	4.47	2.27	5.67	0.25	VMS
V-11	Ashele	Habahe	Xinjiang	Hercynian	1.83	43.80	109.50	2.00	VMS
V-12	Tiemierteduo	Aletai	Xinjiang	Hercynian	0.93	11.00	27.50	0.26	VMS
V-13	Abagong	Aletai	Xinjiang	Hercynian	75.00	15.26	38.15	28.61	VMS
V-14	Laochang	Lanchang	Yunnan	Hercynian	0.63	32.86	82.15	0.52	VMS

Additional reference, Dai et al., 2005.

Table 3
HgT concentrations in MVT zinc deposits.

Deposit no.	Deposit name	Locations	Provinces	Host ages	HgT (μg/g)	Zn (10^4 tons)	ZC (10^4 tons)	MR (t)	Deposit types
M-1	Chaihe	Kaiyuan	Liaoning	Yanshanian	1050.00	39.15	97.88	1027.69	MVT
M-2	Qingchengzi	Fengcheng	Liaoning	Yanshanian	10.00	34.93	87.33	8.73	MVT
M-3	Qixiashan	Nanjing	Jiangsu	Yanshanian	2.61	75.5	188.75	4.93	MVT
M-4	Ganjiaxiang	Nanjing	Jiangsu	Yanshanian	7.02	37.06	92.65	6.50	MVT
M-5	Yinshan	Yangxin	Hubei	Yanshanian	0.76	35.49	88.73	0.67	MVT
M-6	Limei	Huayuan	Hunan	Yanshanian	17.60	153.26	383.15	67.43	MVT
M-7	Chaiqing	Lengshuijiang	Hunan	Indosinian	12.10	35.83	89.58	10.84	MVT
M-8	Houjiangqiao	Daoxian	Hunan	Yanshanian	2.13	50.8	127.00	2.71	MVT
M-9	Beishan	Huanjiang	Guangxi	Yanshanian	77.4	103.33	258.33	199.94	MVT
M-10	Siding	Rongan	Guangxi	Yanshanian	8.51	44.19	110.48	9.40	MVT
M-11	Laochang	Yangshuo	Guangxi	Yanshanian	10.00	14.3	35.75	3.58	MVT
M-12	Guli	Wuxuan	Guangxi	Yanshanian	21.60	9.86	24.65	5.32	MVT
M-13	Zhaiziping	Kangding	Sichuan	Caledonian	127.00	26.61	66.53	84.49	MVT
M-14	Tianbanshan	Huili	Sichuan	Caledonian	2.11	94.14	235.35	4.97	MVT
M-15	Xiaoshifang	Huili	Sichuan	Caledonian	44.77	29.73	74.33	33.28	MVT
M-16	Daliangzi	Huidong	Sichuan	Caledonian	41.82	200.72	501.8	209.85	MVT
M-17	Zhazichang	Hezhang	Guizhou	Himalayan	2.13	13.36	33.4	0.71	MVT
M-18	701	Huize	Yunnan	Hercynian	7.92	20.8	52.00	4.12	MVT
M-19	Kuangshanchang	Huize	Yunnan	Hercynian	25.20	49.6	124.00	31.25	MVT
M-20	Wuxingchang	Huize	Yunnan	Hercynian	9.71	9.89	24.73	2.40	MVT
M-21	Fule	Luoping	Yunnan	Hercynian	5.15	27.91	69.78	3.59	MVT
M-22	Bainiuchang	Mengzi	Yunnan	Caledonian	0.45	68.74	171.85	0.77	MVT
M-23	Dulong	Maguan	Yunnan	Yanshanian	2.78	241.93	604.83	16.81	MVT

Additional reference, Dai et al., 2005.

Table 4
HgT concentrations in IR zinc deposits.

Deposit no.	Deposit name	Locations	Provinces	Host ages	HgT (μg/g)	Zn (10^4 tons)	ZC (10^4 tons)	MR (t)	Deposit types
IR-1	Pingfeng	Pucheng	Fujian	Yanshanian	0.10	19.49	48.73	0.05	IR
IR-2	Cuiqian	Gaoan	Jiangxi	Yanshanian	0.14	24.54	61.35	0.09	IR
IR-3	Jianai	Datian	Fujian	Yanshanian	0.15	14.91	37.28	0.06	IR
IR-4	Yinkeng	Putian	Fujian	Yanshanian	0.15	16.69	41.73	0.06	IR
IR-5	Shangcang	Longmen	Guangdong	Yanshanian	0.21	22.12	55.3	0.12	IR
IR-6	Yuli	Wuxian	Jiangsu	Yanshanian	0.24	24.18	60.45	0.15	IR
IR-7	Qibaoshan	Shanggao	Jiangxi	Yanshanian	0.28	26.32	65.8	0.18	IR
IR-8	Dachang	Nandan	Guangxi	Yanshanian	0.32	318.44	796.1	2.55	IR
IR-9	Yindong	Fuding	Fujian	Yanshanian	0.32	24.90	62.25	0.20	IR
IR-10	Huangshaping	Guiyang	Hunan	Yanshanian	0.34	110.8	277.00	0.94	IR
IR-11	Shuikoushan	Changning	Hunan	Yanshanian	0.36	111.08	277.70	1.00	IR
IR-12	Caijiayingzi	Zhangbei	Hebei	Yanshanian	0.39	143.96	359.9	1.40	IR
IR-13	Chaipai	Longmen	Guangdong	Indosinian	0.44	34.63	86.58	0.38	IR
IR-14	Lengshuikeng	Guixi	Jiangxi	Yanshanian	0.46	218.82	547.05	2.52	IR
IR-15	Xiertala	Chenbaerhu	Neimenggu	Yanshanian	0.59	27.67	69.18	0.41	IR
IR-16	Lame	Nandan	Guangxi	Yanshanian	0.73	56.51	141.28	1.03	IR
IR-17	Qibaoshan	Liuyang	Hunan	Yanshanian	0.95	21.64	54.1	0.51	IR
IR-18	Sanhe	Eergunazuoqi	Neimenggu	Yanshanian	1.31	15.73	39.33	0.52	IR
IR-19	Wangjiazhuang	Fushan	Shandong	Yanshanian	1.55	22.38	55.95	0.87	IR
IR-20	Xiangkuang	Qixia	Shandong	Yanshanian	1.55	15.34	38.35	0.59	IR
IR-21	Huanren	Huanren	Liaoning	Caledonian	1.59	49.59	123.98	1.97	IR
IR-22	Jiaoli	Shangyou	Jiangxi	Yanshanian	1.59	1.01	2.53	0.04	IR
IR-23	Haobugao	Balin	Neimenggu	Yanshanian	1.88	62.46	156.15	2.94	IR
IR-24	Congshuban	Chenzhou	Hunan	Yanshanian	2.13	45.32	113.3	2.41	IR
IR-25	Wubu	Huangyan	Zhejiang	Yanshanian	2.55	88.28	220.7	5.63	IR
IR-26	Tamu	Yingjisha	Xinjiang	Hercynian	3.11	13.43	33.58	1.04	IR
IR-27	Gejiu	Gejiu	Yunnan	Yanshanian	3.27	53.00	132.5	4.33	IR
IR-28	Huoshibulake	Atushi	Xinjiang	Hercynian	3.49	3.69	9.23	0.32	IR
IR-29	Baiyinnuo	Balin	Neimenggu	Yanshanian	4.08	196.04	490.1	20.00	IR
IR-30	Yueshan	Lujiang	Anhui	Yanshanian	4.10	27.56	68.9	2.82	IR
IR-31	Taolin	Linxiang	Hunan	Yanshanian	7.00	65.32	163.3	11.43	IR
IR-32	Xiaoxilin	Yichun	Heilongjiang	Hercynian	7.00	53.00	132.5	9.28	IR
IR-33	Changtun	Daxin	Guangxi	Yanshanian	7.04	22.73	56.83	4.00	IR
IR-34	Jiawula	Chenbaerhu	Neimenggu	Yanshanian	8.80	37.90	94.75	8.34	IR
IR-35	Fangniugou	Yitong	Jilin	Hercynian	10.00	35.70	89.25	8.93	IR
IR-36	Quli	Lushi	Henan	Yanshanian	13.54	68.47	171.18	23.18	IR
IR-37	Xialadi	Lincang	Gansu	Hercynian	30.80	0.08	0.20	0.06	IR
IR-38	Qingshuitang	Qidong	Hunan	Yanshanian	41.04	24.20	60.50	24.83	IR
IR-39	Bajiazi	Jianchang	Liaoning	Yanshanian	50.00	22.59	56.48	28.24	IR
IR-40	Shiduolong	Xinghai	Qinghai	Indosinian	50.00	11.11	27.78	13.89	IR
IR-41	Xiaoyingzi	Wengniute	Neimenggu	Yanshanian	67.30	20.48	51.20	34.46	IR
IR-42	Dajianshan	Lianping	Guangdong	Yanshanian	81.60	27.81	69.53	56.73	IR
IR-43	Fozichong	Qinxi	Guangxi	Yanshanian	200.00	33.16	82.90	165.8	IR
IR-44	Yinshan	Dexing	Jiangxi	Yanshanian	308.41	44.34	110.85	341.87	IR

Additional reference, Dai et al., 2005.

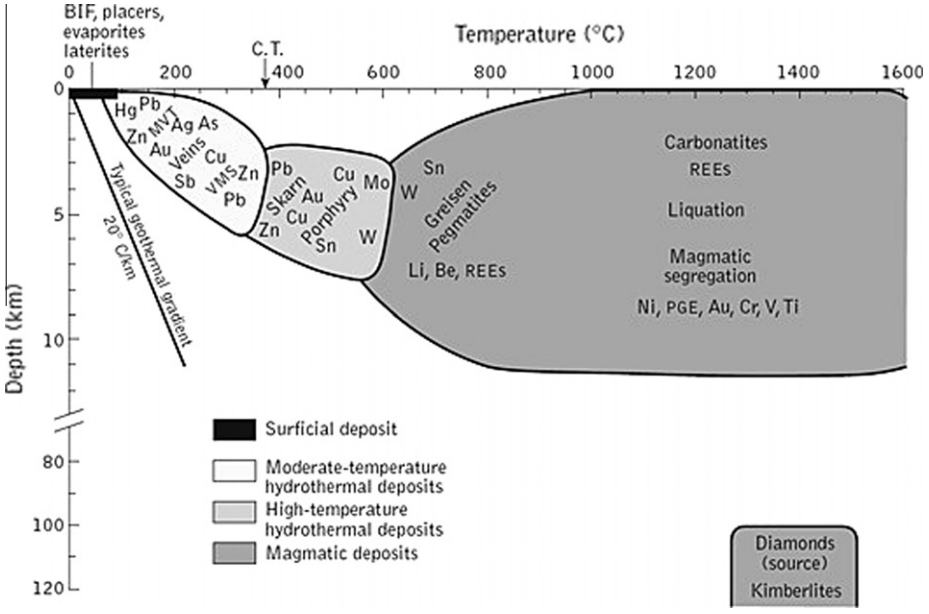

Fig. 2. Pressure and temperature ranges of various ore-forming environments, and the major commodities found in each environment (Edwards and Atkinson, 1986; Evans, 1993). (BIF, banded iron formation; CT, critical temperature of water; MVT, sediment-hosted base metal deposits; REEs, rare-earth elements; PGE, platinum group elements).

Cenozoic metallogeny of western China (Yang, 2000). Numerous giant deposits were formed during this epoch with the best-known example at Jinding, Yunnan, where ore occurs in siliciclastic sediments that were deposited in a rapidly-subsiding Tertiary basin (Zhou et al., 2007; Xue et al., 2007; Hou et al., 2007).

2.2. Sampling sites and Zn ore type classification

As shown in Fig. 1, Zn concentrates from 100 Zn deposits were collected. At each sampling site, a composite sample composed of five sub-samples was collected. During the sampling campaign, all collected samples were stored in sealed polyethylene bags to avoid cross contamination. In the laboratory, samples were homogenized, and sieved to minus 100 mesh prior to digestion. The sampling locations, ore types, the geneses and Zn reserves of each deposit in this study are given in Tables 1–4.

Mineralization occurs in a variety of environments in the Earth's crust as shown in Fig. 2. Mineral deposits form where ore minerals are concentrated and precipitated from magmas or fluids in response to changes in pressure, temperature, and chemical environment. These various processes lead to the formation of elemental associations that are characteristic of the various geological environments. Basically, it is difficult to classify all of the Zn deposits into currently available deposit models (Large, 2004). Keeping these aspects in mind, in this study, for convenience, economically valuable deposits of Zn are classified according to the processes of their formation and are described in Section 3.1.

2.3. Total mercury analysis

In the laboratory, all Zn concentrates were digested with aqua regia in a microwave oven. Mercury concentration was determined using BrCl oxidation and $SnCl_2$ reduction coupled with cold vapor atomic absorption spectrometry, with a detection limit of 0.1 μg L^{-1} (Li et al., 2005). All the samples were analyzed in triplicate. Accuracy was assessed using the certified reference material GBW07168 (CRM Zn concentrate, Institute of Geophysical and Geochemical Exploration, China). The average HgT of GBW07168 was 560 ± 80 μg g^{-1} (n = 5), which is comparable with the certified value of 547 ± 92 μg g^{-1}.

3. Results and discussion

3.1. HgT variations in Zn ore deposit types

Results of HgT in ZCs in China are listed in Tables 1–4. As shown in Fig. 3, the HgT in the ZCs showed a significant variation between the different Zn deposit sub-types. The HgT distribution for SEDEX, VMS, MVT and IR types of deposits departs from a normal distribution and usually approaches a log-normal distribution.

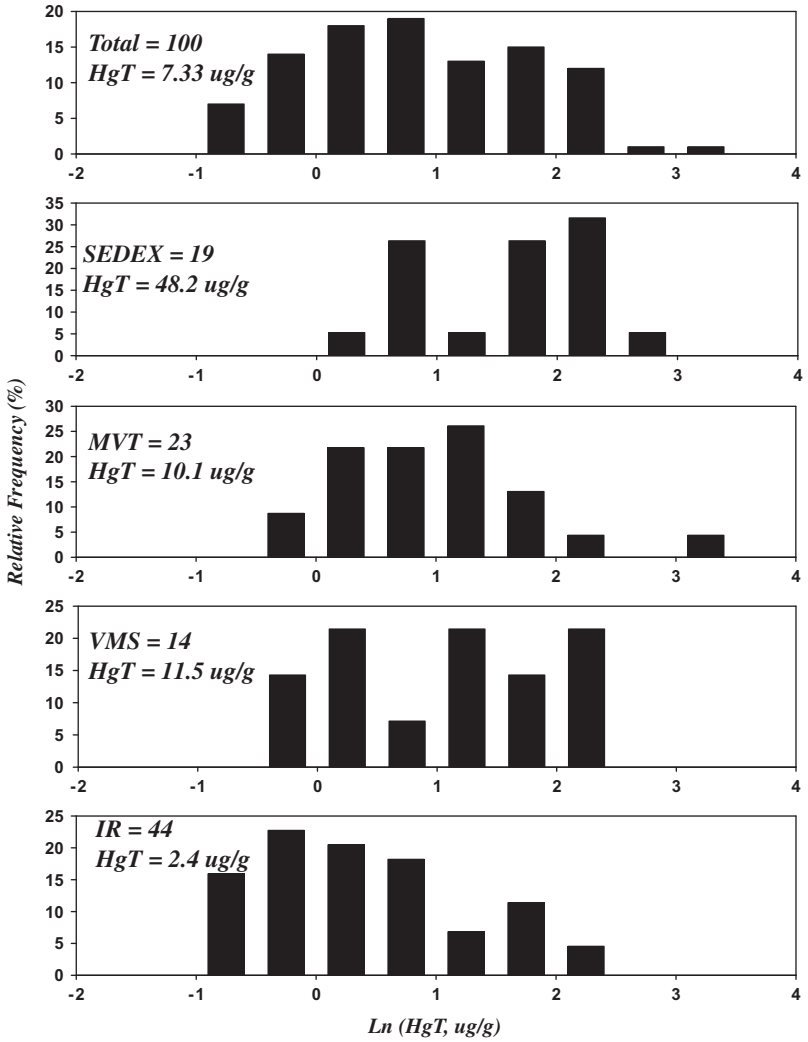

Fig. 3. Histograms showing HgT concentrations for the main classes of Zn deposits.

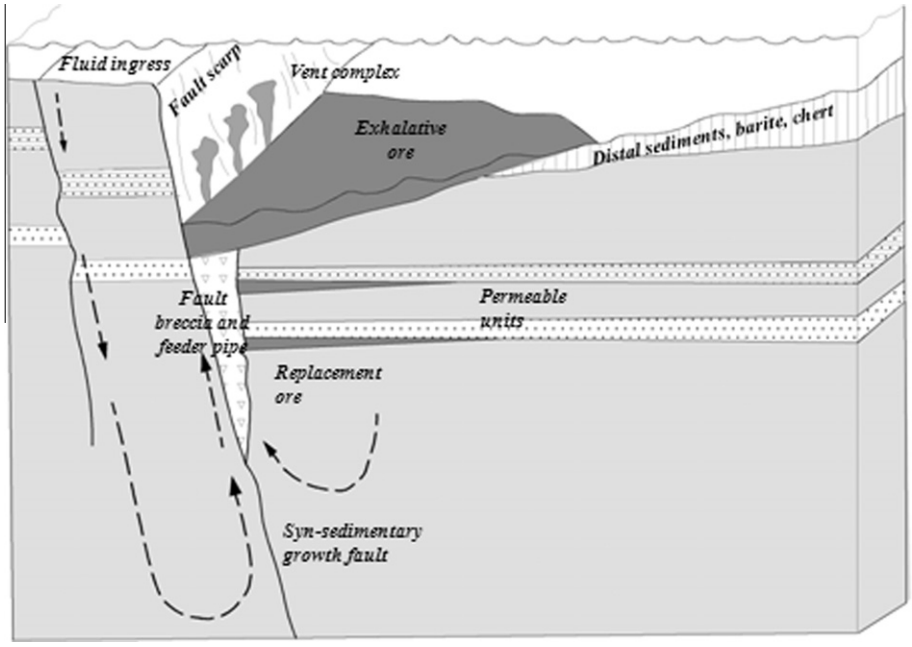

Fig. 4. A generic SEDEX-type deposit model (based on Wilkinson et al., 2005).

Here, the geometric mean is used for comparing the various deposit types.

3.1.1. Sedimentary-exhalative deposits

As shown in Fig. 4, SEDEX is a type of ore deposit which is interpreted to have been formed by the release of ore-bearing hydrothermal fluids into ocean water, where the heavy, hot brines flow mixed with the cooler sea water, resulting in the precipitation of stratiform ore (Cameron, 1975; Leach et al., 2005). Important SEDEX deposits in China are listed in Table 1. SEDEX deposits have the highest geometric mean HgT concentration (48.2 μg/g, n = 19). In previous studies, it has been estimated that Hg resources associated with a SEDEX Zn deposit could reach the reserve of a large-scale Hg deposit (Rytuba, 2003). Huang (1990) demonstrated that in the Fankou SEDEX deposit, the associated Hg occurs only in sphalerite (ZnS), of which the average Hg concentrations reached 790 μg/g and it most probably occurs both as an isomorphic mixture and as micro-inclusions of Hg sulfide. Similarly, Schwartz (1997) also summarized the HgT of Zn deposits and concluded that SEDEX deposits have the highest Hg content ranging from 27 to 1198 μg/g Hg. Thus, SEDEX deposits are characterized by an enriched Hg contents.

It is possible that the elevated HgT levels in SEDEX deposits could be explained by the relatively higher HgT in sediments. The source of metals and mineralizing solutions for SEDEX deposits is from deep formational brines. Deep formational brines are defined as saline to hypersaline waters which are produced from sediments during diagenesis (Leach et al., 2005). Metals such as Pb, Zn and Hg are often enriched in sediments (WHO, 1989). Those elements originated from the water in which the sediments were originally deposited, and were precipitated with sulfides or adsorbed to the organic materials (Jeng, 1992). For example, dissolved Hg has a strong affinity for organic matter and suspended sediment and, therefore, could be expected to be bound to these particles in the water column and subsequently accumulate in sediments. The relative enrichment of metals in sediment is even more marked in some organic-rich black shales, which may hold a large amount of Zn, Pb and Hg bound to clay minerals, organic residues and sulfides. Average Hg levels are reported to be higher in shale (400 μg kg^{-1}) compared to the average concentrations in crustal rocks that is probably less than 80 μg kg^{-1} (Tauson and Abramovich, 1980).

Here, it is stressed that such associations cannot only lead to higher concentrations of Hg in these types of rock units but also in the transport of Hg away from the sites of sediment accumulation (White, 1967). During diagenesis, metals are liberated from clay and carbonate minerals as the mineralogy changes, and the remaining pore fluid becomes concentrated into what is known as deep formational brine. The solution of metals, salts and water produced by diagenesis is produced at temperatures between 150 and 350 °C. Hydrothermal fluid compositions are estimated to have a salinity of up to 35% NaCl with metal concentrations of 5–15 μg/g Zn and Pb. A large amount of Hg might be able to be carried in solution because of the high salinity (Fein and Williams-Jones, 2009). Generally these formational brines also carry a considerable amount of S (Kelley et al., 1995).

3.1.2. Volcanogenic massive sulfide deposits

VMS is a type of metal sulfide (mainly Zn–Pb–Cu) ore deposit, in which the mineralization is associated with the thick sedimentary sequences. VMS deposits are related to intrusion by volcanic edifices in submarine environments, and are formed by hydrothermal circulation and exhalation of sulfides. This separates VMS deposits from SEDEX deposits. Hydrothermal circulation is generally considered to be driven via heat in the crust often related to deep-seated intrusions (Eckstrand et al., 1996). Selected VMS deposits in China are listed in Table 2. The study showed that VMS deposits have intermediate HgT concentration of 11.5 μg/g (n = 14), which suggests that VMS deposits potentially can contain sufficient Hg to be of environmental concern. The most Hg enriched VMS deposits have been reported in the Skellefte district, Sweden where over 85 deposits are present which commonly have ores containing from 10 to 340 μg/g of Hg (Allen et al., 1997).

Mercury is found in abundance in VMS deposits associated with subaerial and submarine volcanism. Mercury minerals are generally not present in VMS deposits, and Hg is primarily present in solid solution within sphalerite, which can contain up to 41.1 wt.% Hg in its structure (Tauson and Abramovich, 1980). According to

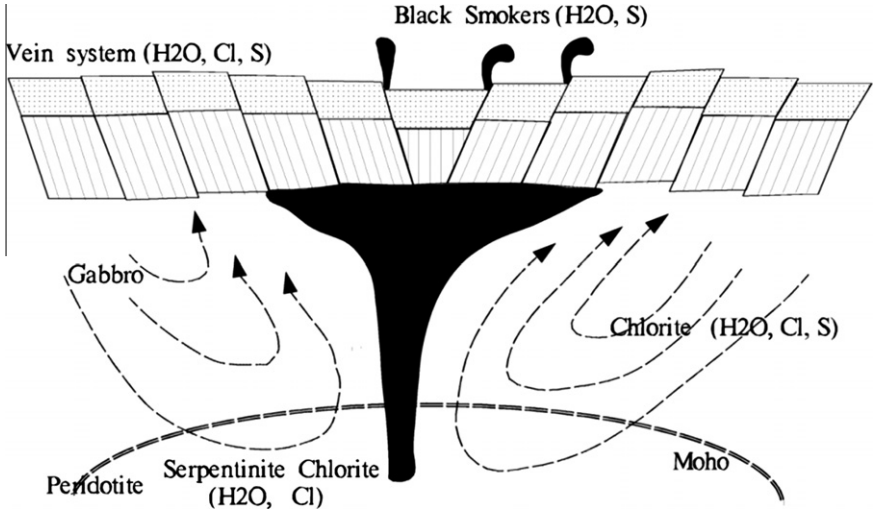

Fig. 5. A generic VMS type deposit model (Gregory and Taylor, 1981).

common concepts, as shown in Fig. 5, the source of metal and S in VMS deposits is a combination of incompatible elements which are concentrated in the fluid phase of a volcanic eruption and metals leached from the alteration zone due to hydrothermal circulation (Eckstrand et al., 1996). Natural Hg arises from the degassing of the Earth's crust through volcanic gases. Much higher Hg levels (up to 1500 μg kg^{-1}) have been found in eclogite and peridotite in inclusions in kimberlite pipes, suggesting that the deep crust and upper mantle may be considerably enriched in Hg compared to the upper crustal rocks (Greenwood and Earnshaw, 1984). The transport of metals occurs via convection of hydrothermal fluids, the heat for this being supplied by the magma chamber which sits below the volcanic edifice, which can also enrich the hydrothermal fluid in S and metal ions. Submarine volcanism and coeval chemical sedimentation may have provided a favorable setting for Hg transport and fixation (Schwartz, 1997). VMS deposits are currently being formed by hydrothermal processes along submarine divergent margins (e.g. mid-ocean ridges and back arc rifts) (Herzig and Hannington, 1995). The sulfurous plumes known as the black smokers deposit a variety of metal sulfides as the hot hydrothermal solutions meet and mix with deep ocean water. A recent study has documented the deposition of Hg in sea-floor hydrothermal settings (Stoffers et al., 1999), indicating that mid-ocean ridge systems may be important sources of Hg to the oceans. Elevated concentrations of Hg in submarine hydrothermal fluids, ranging from 4 to 16 pM have also been documented (Lamborg et al., 2006).

3.1.3. Mississippi valley type

Mississippi Valley-Type deposits (MVTs), being first recognized along the Mississippi River Valley in the USA, are hydrothermal Zn ore deposits that are characterized by (1) low-temperature formation (50–200 °C), (2) epigenetic emplacement within restricted carbonate strata of sedimentary basins, and (3) precipitation from highly saline brines (Sangster, 1995; Misra, 1999;Leach et al., 2001). The major MVT deposits in China are listed in Table 3 and the geometric mean HgT is 10.1 μg/g (n = 23).

According to common concepts, MVTs lack a genetic relationship to igneous activity or igneous rocks (Heyl, 1983; Sverjensky, 1986). Similar to SEDEX deposits, the source of S and metals within MVTs is the low-temperature hydrothermal solution formed by diagenetic recrystallization of the carbonates. The brines acquired their metal (such as Pb, Zn, Hg) load along their long travel path through the sedimentary rocks (Schwartz, 1997). The hydrothermal solution normally migrates into stratigraphic highs, such as folds, and typically also concentrates in fault zones at the margins of basement grabens. If the solutions are not trapped successfully within the carbonate host, it is possible for the hydrothermal fluids to leak out into the ocean basin and form SEDEX Zn deposits.

Previous studies have demonstrated that the trap for MVT Zn sulfides occurs as a consequence of S geochemical process and hydrocarbon interactions (Peabody, 1993). Metals such as Pb, Zn and Hg can be absorbed by the hydrocarbons (Fein and Williams-Jones, 2009). The hydrocarbons can either leak out of the fault zone or fold hinge, leaving a stockwork of weakly mineralized carbonate–sulfide veins, or can degrade via pyrolysis in place to form bitumens. Once hydrocarbons are converted to bitumen, their ability to chelate metal ions and S is reduced and results in these elements being expelled into the fluid, which becomes saturated in Zn, Pb, Hg and S. Commonly MVT deposits are formed by the combination of hydrocarbon pyrolysis, which liberates metal ions and S to form an acidic solution. The acidic solution dissolves the host carbonate resulting in the formation of sulfide minerals such as sphalerite and galena. Mercury may be present in sphalerite in solid solution (Rytuba, 2003). In general, Hg exhibits a widespread association with organic material. Mercury–bitumen deposits are among the largest Hg producers (Peabody, 1993). Mercury deposits have certain features in common with MVT deposits: (1) the deposits formed at shallow depths; (2) the ore-forming fluids had low temperatures (usually <200 °C); and (3) hydrothermal aquifers composed of sedimentary rocks played a major role in the ore-forming process.

3.1.4. Intrusion related types

IRs are believed to be genetically related to high-temperature hydrothermal processes that are related to the emplacement of magmatic intrusions. They are responsible for the genesis of several types of ore deposit of economic value. Selected major IR deposits are listed in Table 4. As seen in Fig. 3, IRs are associated with lower Hg concentrations (HgT = 2.4 μg/g, n = 44) than the other deposit types studied. The causes of the generally lower concentrations might be attributed to certain features of the specific IR deposit type. The IRs presented here can be classified into two main types:

(1) *Porphyry-type deposits* are principally mined for Cu, Mo and Sn, but contain subordinate amounts of Pb and Zn, which occur with quartz in a complex network of veinlets or are scattered throughout the host-rocks. Porphyry deposits refer

to disseminated mineralization spatially associated with felsic intrusions in orogenic belts. The dispersion of Hg in the porphyry environment seems to be influenced by the high temperature of ore formation and/or nature of wall–rock alteration. The relatively high temperature at which porphyry deposits form, minerals may lead to an increased mobility and loss of volatiles, including Hg, from the melt. These volatiles are then deposited as the melt cools. Gott and McCarthy (1966), in a study of the porphyry Cu deposits near Ely, Nevada, found that Hg was enriched in rocks surrounding the ore deposits and depleted in the central ore-bearing intrusive rocks. This dispersion pattern was attributed to the higher temperature prevailing in the center of the ore deposit causing Hg to migrate outward, forming a halo around the deposit. Further investigations are needed to determine the concentrations of Hg in porphyry Zn ores.

(2) *Skarn deposits* include carbonate-replacement deposits being related to igneous intrusions, but their genesis involves contact metasomatism of favorable host rocks, most commonly limestone. The ore-forming fluids are derived mainly from the intrusion. The ore bodies are commonly irregular in shape and may terminate abruptly at structural discontinuities. Skarns are generally zoned, with anhydrous minerals closest and hydrous minerals more distal to the intrusion. Base-metal sulfides usually occur in the outer parts of a skarn deposit. This zonal sequence reflects the differences in temperature and in the properties of the metals in solution. Because Hg and many of its compounds are highly volatile, there is a widespread belief that Hg is readily lost from skarn deposits. The presence of high temperature in the fluid phase, the piercement structures, and sulfide-bearing veins may serve as pathways for volatile Hg to be mobilized, redeposited, and/or lost during skarn deposit formation. Perhaps this is an important mechanism having the capability of producing Hg haloes around IR deposits (Olade and Fletcher, 1976).

3.2. Evaluation of potential environmental impact of Zn smelting in China

Mercury is present in several types of Zn deposits at concentrations sufficient to make many of these ore deposits a potentially significant source of Hg emissions to the environment. In these deposits, Hg is released primarily in stack gases during the roasting or smelting of massive sulfide ores (Rytuba, 2003). In China, the high demand for Zn metal brought about by rapid industrialization has resulted in Zn mineral-processing with limited regulations on Hg emissions. Consequently, Hg continues to be released to the atmosphere as a result of China's large Zn production (Jiang, 2004; Feng et al., 2004).

3.2.1. Evaluation of Hg reserves in Zn deposits in China

To evaluate the potential environmental impact of Zn smelting and refining processes in China, the basic data on Zn production were acquired from a Zn concentrate market study as shown in Tables 1–4 (Dai et al., 2005).

As supposed by previous studies, Hg occurs only in ZC and Chinese ZC has a Zn concentration of 40 wt.% (Li et al., 2010; Schwartz, 1997; Dai et al., 2005). Thus, the Hg reserve of deposit *ij* (HgR_{ij}, in tons) could be calculated as follows:

$$HgR_{ij} = \frac{Zn_{ij} \times 10^{-2}}{40\%} \cdot HgT_{ij} \quad (1)$$

where *i* indicates four sub-types of Zn deposits representing the MVT ($i = m$),SEDEX ($i = s$), VMS ($i = v$) and IR ($i = r$) as shown in Tables 1–4. The symbol *j* represents the deposit number of four sub-types of Zn deposits [MVT (j = 1–23), SEDEX (j = 1–19), VMS (j = 1–14) and IR (j = 1–44)]. The Zn_{ij} and HgT_{ij} represent the total Zn reserve (in units of 10^4 tons) and the geometric mean HgT (units in mg/kg) of deposit *ij*, respectively. The Zn_{ij} data in the study were obtained from literature (Dai et al., 2005).

According to Eq. (1), the total Hg reserve (HgR, in tons) and the total Zn reserve of Zn (ZnR, in 10^4 tons) in the 100 Zn deposits were established as follows:

$$ZnR = \left(\sum_{j=23} Zn_{ij}^{i=m} + \sum_{j=19} Zn_{ij}^{i=s} + \sum_{j=14} Zn_{ij}^{i=v} + \sum_{j=44} Zn_{ij}^{i=r}\right) \quad (2)$$

$$HgR = \left(\sum_{j=23} HgR_{ij}^{i=m} + \sum_{j=19} HgR_{ij}^{i=s} + \sum_{j=14} HgR_{ij}^{i=v} + \sum_{j=44} HgR_{ij}^{i=r}\right) \quad (3)$$

Thus, based on Eqs. (1)–(3), the fraction of the Zn reserve (FZn_i) and Hg reserve (FHg_i) of a four sub-type Zn deposit in China could be calculated by:

$$FZn_i(\%) = \frac{\sum ZnR_{ij}^{i=m,s,v,r}}{ZnR} \cdot 100\% \quad (4)$$

$$FHg_i(\%) = \frac{\sum HgR_{ij}^{i=m,s,v,r}}{HgR} \cdot 100\% \quad (5)$$

Based on Eq. (2), the ZnR of the 100 Zn deposits is 78.9 Mt, which consisted 81% of the total Zn reserve (97.8 Mt in 2002) in China (Dai et al., 2005). Using Eq. (4), it was found that the SEDEX type accounts for 44.6% of the Zn reserves in China and it is the most important ore type for Zn mineralization in China followed by MVT (17.9%), IR (28.9%) and VMS (8.6%) (Fig. 6A).

Based on Eq. (3), the by-product Hg reserve in the 100 Zn deposits is established to be 12,263 tons. The relative contribution of the four sub-types of Zn deposit were calculated by Eq. (5) and are shown in Fig. 6B, the largest by-product Hg comes from SEDEX (70.9%), followed by MVT (14.2%), VMS (8.5%), and IR (6.4%) deposits. The total Hg reserves from some of the most Hg-enriched SEDEX deposits, such as Fankou (~3000 tons), are comparable to those of a moderate size Hg deposit.

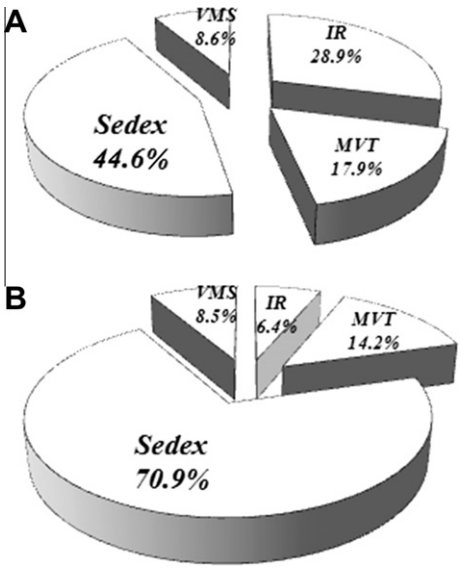

Fig. 6. Percentage of estimated Zn reserves (A) and Hg contribution (B) for Zn deposits from four sub-types of Zn deposits in China.

3.2.2. Evaluation of Hg emissions during Zn smelting in China

Broadly speaking, Zn extraction from ZCs can be divided into hydrometallurgical and pyrometallurgical techniques (Li et al., 2010; Fugleberg, 1999; Hylander and Herbert, 2008). In China, nearly all hydrometallurgical and pyrometallurgical techniques require roasting of sulfide minerals for desulfurization (Jiang, 2004). In the roasting furnace, O_2 reacts with ZCs at a temperature of about 900–1000 °C, producing Zn oxides and releasing sulfur SO_2 as well as other volatile compounds (e.g., Hg025) (Fugleberg, 1999). Sulfur in SO_2, which has an economic value as a byproduct, may be recovered as elemental S, liquid SO_2, gypsum, or H_2SO_4. For gases with a SO_2 concentration in excess of 1%, S is often recovered in a H_2SO_4 plant (SAP). In China, up to 80% of Zn smelters have installed SAPs (Song et al., 2010). There may be two mechanisms through which Hg can be taken up by H_2SO_4, (1) the H_2SO_4 can oxidize Hg *in situ* (Habashi, 1978), and (2) Hg can be oxidized by the V_2O_5 catalyst bed in the acid plant, which is utilized for conversion of SO_2 to SO_3 (Li et al., 2010). When SO_2 and Hg^0 vapor are carried through SAP, a fraction of the Hg vapor is retained by the SAP (Hg recovery efficiency of 95%), while the rest is emitted into the atmosphere. However, 20% of Zn smelters do not have a SAP, in which case the Hg recovery efficiency is >10% (Song et al., 2010). Thus, for Zn smelters, the Hg emission factor (α) mainly depends on whether a SAP is utilized or not, and an average Hg emission factor is calculated with the following equation:

$$\alpha = (80\% \cdot 5\% + 20\% \cdot 90\%) = 22\% \quad (6)$$

Then, the annual Hg emission ($Hg_{emission}$) from Zn smelting in China was calculated as follows:

$$Hg_{emission} = Zn_{an} \cdot \frac{HgR}{ZnR} \cdot \alpha \quad (7)$$

where Zn_{an} represents the annual production of Zn in China. The Zn_{an} is increasing dramatically, from 2.16 million tons in 2002 to 3.15 million tons in 2006 with an average annual increase of 8.9% (ECCNMY, 2003–2007).

According to Eq. (6), the annual Hg emission ($Hg_{emission}$) from Zn smelting in China was 107.7 tons in 2006. A few studies have evaluated annual Hg emissions from Zn smelting processes in China. Based on the mass balance method, the inventory of Hg emissions from industrial-scale Zn production plants in China were established to be from 80.7 to 104.2 tons during 2002 to 2006 (Li et al., 2010; Feng et al., 2004). The literature data are comparable to the present estimate.

4. Conclusions

Mercury occurs as trace to recoverable amounts in many types of Zn ores, depending on ore type and genesis. This study suggested that: (1) SEDEX deposits have the highest HgT concentrations. The reason may be due possibly to the relative higher Hg background in sediments providing the ore-forming fluid; (2) VMS and MVT deposits have moderate HgT concentrations. VMS deposits probably received their Hg from an input of Hg from a mantle source. However, the source of metals within MVTs may be the low-temperature hydrothermal solution formed by diagenetic recrystallization of the carbonates; (3) IRs have the lowest HgT. The high temperature in the fluid phase and the piercement structures of IRs may result in loss of Hg during Zn mineralization. It has been demonstrated that the sources and/or geochemical processes that form a particular type of mineral deposit can result in loss or concentration of Hg in mineral phases that are specific to the mineral deposit type. The findings presented here may be useful in evaluating their potential usefulness in detailed geochemical exploration.

Zinc smelters produced 3.15 million tons of Zn from ore concentrates in China in 2006 (ECCNMY, 2003–2007). This could have resulted in the emission of 108 tons of Hg to the atmosphere. The largest amount of Hg emission comes from processing SEDEX ores (70.9%), followed by MVT (14.2%), VMS (8.5%) and IR (6.4%) deposits.

Acknowledgements

This research was funded by Natural Science Foundation of China (40825011) and State Environmental Protection Commonweal Trade Scientific Research in China (200909024). We would like to thank Dr. Ron Fuge, Dr. Wang, and the two anonymous reviewers for their thoughtful suggestions.

References

Allen, R.L., Weihed, P., Svenson, S.A., 1997. Setting of Zn–Cu–Au–Ag massive sulfide deposits in the evolution and facies architecture of a 1.9 Ga marine volcanic arc, Skellefte district, Sweden. Econ. Geol. 91, 1022–1053.

Cameron, E.M., 1975. Geochemical methods of exploration for massive sulphide mineralization in the Canadian Shield. Geochemical Exploration, vol. 44. Elsevier, Amsterdam, pp. 21–49.

Dai, Z.X., Sheng, J.F., Bai, Y., 2005. Distribution and Potentiality of Lead and Zn Resources in the World. Earthquake Publishing (in Chinese).

Editorial Committee of China Nonferrous Metals Yearbook (ECCNMY), 2003–2007. China Mechanical Industry Yearbook 2003–2007. China Nonferrous Metals Industry Association Press, Beijing (in Chinese).

Eckstrand, O.R., Sinclair, W.D., Thorpe, R.I., 1996. Geology of Canadian Mineral Deposit Types. Decade in North American Geology, vol. 8, Geol. Surv. Canada, P-1, pp. 129–196.

Edwards, R., Atkinson, K., 1986. Ore Deposit Geology. Chapman and Hall, London.

Evans, A.M., 1993. Ore Geology and Industrial Minerals: An Introduction. Blackwell Scientific Publications, Oxford.

Fedikow, M.A.F., Amor, S.D., 1990. Evaluation of a mercury-vapour detection system in base- and precious-metal exploration, northern Manitoba. J. Geochem. Explor. 38, 351–374.

Fein, J.B., Williams-Jones, A.E., 2009. The role of mercury-organic interactions in the hydrothermal transport of mercury. Econ. Geol. 92, 20–28.

Feng, X.B., Li, G.H., Qiu, G.L., 2004. A preliminary study on mercury contamination to the environment from artisanal zinc smelting using indigenous methods in Hezhang county, Guizhou, China – Part 1: Mercury emission from zinc smelting and its influences on the surface waters. Atmos. Environ. 38, 6223–6230.

Fugleberg, S., 1999. Finnish Expert Report on Best Available Techniques in Zinc Production, The Finnish Environment, Report 315. Finnish Environment Institute, Helsinki.

Fursov, Z.Y., 1958. Haloes of dispersed mercury as prospecting guides at the Aehisai lead–zinc deposits. Geochemistry 338, 344.

Garrett, R.G., 1974. Mercury in some granitoid rocks of the Yukon and its relation to gold–tungsten mineralization. J. Geochem. Explor. 3, 277–290.

Gott, O.B., McCarthy, A.H.Jr., 1966. Distribution of gold, silver, tellurium and mercury in the Ely Mixiing District, White Pine County, Nevada. US Geol. Surv. Circ. 5, 535.

Greenwood, N.N., Earnshaw, A., 1984. The Chemistry of Elements. Oxford.

Gregory, R.T., Taylor Jr., H.P., 1981. An oxygen isotope profile in a section of Cretaceous oceanic crust, Samail Ophiolite, Oman: evidence for $\delta^{18}O$-buffering of the oceans by deep (>5 km) seawater-hydrothermal circulation at mid-ocean ridges. J. Geophys. Res. 86, 2737–2755.

Habashi, F., 1978. Metallurgical plants: how mercury pollution is abated. Environ. Sci. Technol. 12, 1372–1376.

Herzig, P.M., Hannington, M.D., 1995. Polymetallic massive sulfides at the modern seafloor – a review. Ore Geol. Rev. 10, 95–115.

Heyl, A.V., 1983. Geologic characteristics of three major Mississippi Valley type districts. In: Kisvarsanyi, G., Grant, S.K., Pratt, W.P., Koenig, J.W. (Eds.), Proc. Internat. Conf. Mississippi Valley Type Lead–Zinc Deposits. University of Missouri-Rolla Press, Rolla, pp. 27–60.

Holland, H.D., 1972. Granites, solutions and base metal deposit. Econ. Geol. 67, 281–301.

Hou, Z., Zaw, K., Pan, G., Mo, X., Xu, Q., 2007. Sanjiang Tethyan metallogenesis in S.W. China: tectonic setting, metallogenic epochs and deposit types. Ore Geol. Rev. 31, 48–87.

Huang, H.L., 1990. The occurrence character of associated mercury in Fankou Lead–Zinc Deposit, Guangdong. Geology 1 (5), 14–21 (in Chinese).

Hylander, L.D., Herbert, R.B., 2008. Global emission and production of mercury during the pyrometallurgical extraction of nonferrous sulfide ores. Environ. Sci. Technol. 42, 5971–5977.

Jeng, A.S., 1992. Weathering of some Norwegian Alum Shales: II. Laboratory simulations to study the influence of aging, acidification and liming on heavy metal release. Acta Agric. Scand., Sect. B, Soil Plant Sci. 42, 76–87.

Jiang, J.M., 2004. Status and sustainable development of lead and zinc smelting industry in China. Chin. J. Nonferrous Met. 14 (S1), 52–62.

Kelley, K.D., Seal, R.R., Schmidt, J.M., Hoover, D.B., Klein, D.P., 1995. Sedimentary exhalative Zn–Pb–Ag deposits. In: du Bray, E.A. (Ed.), Preliminary Compilation of Descriptive Geoenvironmental Mineral Deposit Models. US Geol. Surv. Open File Rep. 95-831, pp. 225–233.

Kilinc, I.A., Burnham, C.W., 1972. Partitioning of chloride between a silicate melt and co-existing aqueous phase from 2 to 8 kilobars. Econ. Geol. 67, 231–235.

Lamborg, C.H., Von Damm, K.L., Fitzgerald, W.F., Hammerschmidt, R.Z., 2006. Mercury and monomethylmercury in fluids from Sea Cliff submarine hydrothermal field, Gorda Ridge. Geophys. Res. Lett. 33, L17606.

Large, R.R., 2004. SEG Presidential Address: Ore Deposit Models, the Deposit Spectrum and Hybrid Ore Deposits. Predictive Mineral Discovery under Cover. SEG Conference, 27 September–1 October, 2004, Perth, Australia, Centre for Global Metallogeny. The University of Western Australia, Publication, vol. 33, pp. 162–164.

Leach, D.L., Bradley, D.C., Lewchuck, M., Symons, D.T.A., Brannon, J., de Marsily, G., 2001. Mississippi Valley-type lead–zinc deposits through geological time: implications from recent age-dating research. Miner. Deposita 36, 711–740.

Leach, D.L., Sangster, D.F., Kelley, K.D., Large, R.R., Garven, G., Allen, C.R., Gutzmer, J., Walters, S., 2005. Sediment-hosted lead–zinc deposits: a global perspective. In: Henquist, J., Thompson, J., Richards, J.G. (Eds.), SEG 100th Anniversary Special Publication.

Li, Z.G., Feng, X.B., He, T.R., 2005. Determination of total mercury in soil and sediment by aquaregia digestion in the water bath coupled with cold vapor atom fluorescence spectrometry. Bull. China Soc. Mineral Petrol. Geochem. 24 (2), 140–143 (in Chinese).

Li, G.H., Feng, X.B., Li, Z.G., Qiu, G.L., Shang, L.H., Liang, P., Wang, D.Y., Yang, Y.K., 2010. Mercury emission to atmosphere from primary Zn production in China. Sci. Total Environ. 408, 4607–4612.

McCarthy, J.H., 1972. Mercury vapour and other volatile components in the air as guides to ore deposits. J. Geochem. Explor. 1, 143–162.

Misra, K.C., 1999. Understanding Mineral Deposits. Kluwer Academic Publishers, Boston, MA.

Nelson, C.E., 1990. Comparative geochemistry of jasperoids from Carlin-type gold deposits of the western United States. J. Geochem. Explor. 36, 171–195.

Nriagu, J.O., Pacyna, J.M., 1988. Quantitative assessment of worldwide contamination of air, water and soils by trace metals. Nature 333, 134–139.

Olade, M.A., Fletcher, W.K., 1976. Trace element geochemistry of the Highland Valley and Guichon Creek Batholith in relation to porphyry copper mineralization. Econ. Geol. 71, 733–748.

Ozerova, N.A., Rusinov, V.L., Ozerov, Y.K., 1975. The mercury in sulfide deposits emplaced in volcanic suites. Miner. Deposita 10, 228–233.

Pacyna, E.G., Pacyna, J.M., Steenhuisenc, F., Wilson, S., 2006. Global anthropogenic mercury emission inventory for 2000. Atmos. Environ. 40, 4048–4063.

Peabody, C.E., 1993. The association of cinnabar and bitumen in mercury deposits of the California Coast Ranges. In: Parnell, J., Kucha, H., Landais, P. (Eds.), Bitumen in Ore Deposits. Springer, Berlin, pp. 178–209.

Ren, J.S., Chen, T., Niu, Z., 1990. Tectonic Evolution and Mineralization of the Continental Lithosphere in Eastern China and Adjacent Regions. Academic Press, Beijing.

Rytuba, J.J., 2003. Mercury from mineral deposits and potential environmental impact. Environ. Geol. 43, 326–338.

Sangster, D.F., 1995. Mississippi Valley-type lead–zinc. In: Eckstrand, O.R., Sinclair, W.D., Thorpe, R.I. (Eds.), Geology of Canadian Mineral Deposit Types. Geological Survey of Canada, Ottawa, pp. 253–261.

Schwartz, M.O., 1997. Mercury in zinc deposits: economic geology of a polluting element. Int. Geol. Rev. 39, 905–992.

Shen, Y., 2000. Introduction. In: Cheng, Y. (Ed.), Concise Regional Geology of China. Geological Publishing House, Beijing, China, pp. 1–14.

Song, J.X., Wang, S.X., Li, G.H., 2010. Spatial distribution of mercury content of zinc concentrates in China. Sciencepaper Online 6 (5), 472–475.

Stoffers, P., Hannington, M., Wright, I., Herzig, P., Ronde, C. de, 1999. Elemental mercury at submarine hydrothermal vents in the Bay of Plenty, Taupo volcanic zone, New Zealand. Geology 10, 931–934.

Streets, D.G., Hao, J., Wu, Y., Jiang, J., Chan, M., Tian, H., 2005. Anthropogenic mercury emissions in China. Atmos. Environ. 40, 7789–7806.

Sverjensky, D.A., 1986. Genesis of Mississippi Valley-type leadzinc deposits. Ann. Rev. Earth Planet. Sci. 14, 177–199.

Tauson, V.L., Abramovich, M.G., 1980. Hydrothermal study of the ZnS–HgS system. Geochem. Int. 7, 117–128.

Wang, B.X., 1993. Map of volcanic rock Geology of China (1: 1800,000) and its guide. In: Volcanic Rocks. Volcanism and Related Mineral Resources. Geological Publishing House, Beijing, pp. 17–23.

White, D.E., 1967. Mercury and base-metal deposits with associated thermal and mineral waters. In: Barnes, H.L. (Ed.), Geochemistry of Hydrothermal Ore Deposits. Holt, Rinehart and Winston, New York, pp. 575–631 (Chapter 13).

WHO, 1989. Environmental Health Criteria. No. 86-Mercury-Environmental Aspects. World Health Organization, Geneva.

Wilkinson, J.J., Weiss, D.J., Mason, T.F.D., Cores, B.J., 2005. Zinc isotope variation in hydrothermal systems: preliminary evidence from the Irish Midlands ore field. Econ. Geol. 100, 583–590.

Xue, C., Zeng, R., Liu, S., Chi, G., Qing, H., Chen, Y., Yang, J.S., Wang, D., 2007. Geologic, fluid inclusion and isotopic characteristics of the Jinding Zn–Pb deposit, western Yunnan, South China: a review. Ore Geol. Rev. 31, 337–359.

Yang, K., 1998. A plate reconstruction of the eastern Tethyan orogenic belt in southwestern China. In: Flower, M.F.J., Chung, S.L., Lo, C.H., Lee T.Y., Uyeda, S. (Eds.), Mantle Dynamics and Plate Interactions in East Asia. American Geophysical Union, pp. 269–287.

Yang, M., 2000. Basic tectonic framework of China and its evolution. In: Cheng, Y. (Ed.), Concise Regional Geology of China. Geological Publishing House, Beijing, China, pp. 313–339.

You, Y., Li, X., 1990. Research and application of soil–gas mercury surveys for locating deep uranium orebodies. J. Geochem. Explor. 38, 133–143.

Zeng, Y.F., Shen, D.Q., 1987. Stratabound Ore Deposits in Devonian of Nanling district South China. Geological Memoirs Series. Geological Publishing House, Beijing (in Chinese).

Zhai, Y., Deng, J., 1996. Outline of the mineral resources of China and their tectonic setting. Aust. J. Earth Sci. 43, 673–685.

Zhou, T., Yuan, F., Yue, S., Liu, X., Zhang, X., Fan, Y., 2007. Geochemistry and evolution of ore-forming fluids of the Yueshan Cu–Au skarn- and vein-type deposits, Anhui Province, South China. Ore Geol. Rev. 31, 279–303.

Zhu, B., Zhang, J., Zhu, L., Zheng, Y., 1986. Mercury, arsenic, antimony, bismuth and boron as geochemical indicators for geothermal areas. J. Geochem. Explor. 25, 379–388.